The Mars Exploration Rover Suncam[1,2]

Allan R. Eisenman, Carl Christian Liebe, Ramiro Perez
Jet Propulsion Laboratory, California Institute of Technology
4800 Oak Grove Dr, Pasadena CA 91109-8099
818 354 4999, 818 354 7837, 818 354 7921
firstname.lastname@jpl.nasa.gov

Abstract— NASA will send two identical scientific rovers to different locations on Mars in 2003. One of the cameras onboard the rover is called the Pancam. It acquires images of the Sun and determines the sun vector relative to the rover by extracting the centroid of the solar image and processing it. This information is used, in combination with an inclinometer, to point the high gain antenna at Earth and to provide a reference for the inertial measurement unit that is used for rover navigation.

A technical description of the detector, optics and electronics of the Pancam is covered together with a description of the Sun detection/centroiding algorithm. The required accuracy of the Pancam is a fraction of a degree. Therefore, an error budget has been constructed.

Since the angular size of the sun is 0.5 degrees at Earth and 0.35 degrees at Mars, the centroiding algorithms cannot be tested utilizing normal Earth based observations. Consequently, Sun observations are performed at a dedicated solar observing facility. The facility and the measurement of its accuracy are described.

TABLE OF CONTENTS

1. INTRODUCTION

NASA will send two identical scientific rovers to different locations on Mars in 2003. The Rovers will each have a mass of ~150 kg and they will operate for up to 90 days on the surface of Mars. During this period of time, they will travel about 1 km. The primary scientific objective of the mission is to obtain knowledge of ancient water and climate on the red planet. The scientific instruments include a stereo pair of panoramic cameras.

One assignment of the stereo pair of panoramic cameras (Pancams) is to acquire images of the Sun and determine the sun vector relative to the rover by extracting the centroid of the solar image and processing it. This information is used, in combination with an inclinometer, to point the high gain antenna at Earth and to provide a reference for the inertial measurement unit that is used for rover navigation.

The Pancam optics have a field of view of 16° x 16°, an F/# of 20 and an ND5 filter to avoid saturation. A technical description of the detector, optics and electronics of the Pancam is covered, as is the robust Sun detection algorithm.

---

[1] 0-7803-7231-X/01/$10/© 2002 IEEE
[2] IEEEAC paper #273, Updated Sept 19, 2001

The required accuracy of the Pancam is a fraction of a degree. In order to ensure that this is realized, an error budget has been constructed. The error budget includes terms for the CCD read noise, dark current, dark current non-uniformity, pixel response non-homogeneity, charge transfer inefficiency, frame transfer smear, terms for scattered light caused by lens contamination, and terms for ghost images, optical errors, boresight drift and calibration residuals.

The mathematical model of the Pancam that transforms the centroids into angles is discussed. This discussion includes an explanation of how the parameters for the model are found using observations of the real Sun and a 2-axis gimbal.

Since the angular size of the Sun is 0.5° at Earth and 0.35° at Mars, the centroiding algorithms cannot be tested utilizing normal Earth based observations. Therefore, Sun observations are performed at a dedicated solar observing facility at the JPL Table Mountain Observatory, California. This facility uses a coelostat with associated optics that provides an image with Martian characteristics. The facility and the measurement of its accuracy are described.

2. THE MER MISSION

In 2003, two powerful new Mars rovers will be on their way to the red planet. With far greater mobility than the 1997 Mars Pathfinder rover, these robotic explorers will be able to trek up to 100 meters across the surface each Martian day. Each rover will carry a sophisticated set of instruments that will allow it to search for evidence of liquid water that may have been present in the planet's past. The rovers will be identical to each other, but will land at different regions of Mars.

The landing for each will resemble that of the Pathfinder mission. A parachute will deploy to slow the spacecraft, rockets will fire to slow it further just before impact, and airbags will inflate to cushion the landing. Upon reaching the surface, the spacecraft will bounce about a dozen times, and could roll as far as one kilometer (0.6 mile). When it stops, the airbags will deflate and retract and the petals will open up, bringing the lander to an upright position and revealing the rover.

The landed portion of the mission features a design dramatically different from Mars Pathfinder. Where Pathfinder had scientific instruments on both the lander and the small Sojourner rover, these larger rovers will carry all their instruments with them. Immediately after landing, each rover will begin reconnaissance of the landing site by taking a 360-degree visible color and infrared image panorama. Then they will each leave the petal structure behind, driving off to begin exploration.

Using images and spectra taken daily from the rovers, scientists will command the vehicle to go to rock and soil targets of interest and evaluate their composition and their texture at microscopic scales. Initial targets may be close to the landing sites, but later targets can be far afield. These rovers will be able to travel almost as far in one Martian day as the Sojourner rover did over its entire lifetime.

Rocks and soils will be analyzed with a set of five instruments on each rover, and a special device called the rock abrasion tool will be used to expose fresh rock surfaces for study. Each rover has a mass of nearly 150 kilograms (about 300 pounds) and has a range of up to 100 meters per Martian day (sol). Surface operations will last for at least 90 sols, extending to late May 2004, but could continue longer, depending on the health of the vehicles [1]. An artist's image of a MER rover on the Mars surface is shown in Figure 1.

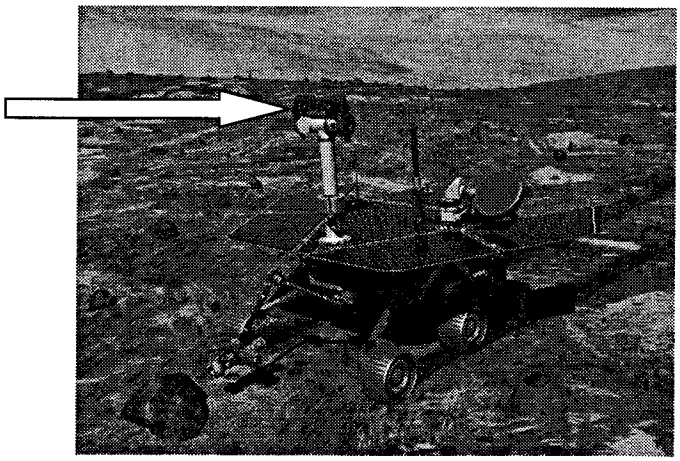

Figure 1. An artist's image of a MER rover on the Mars surface

3. THE PANCAM

One of the cameras on the MER rover is the Pancam. It is indicated with an arrow in Figure 1. The Pancams provide multiple functions in a single instrument package: full 360° azimuth and ±90° elevation gimballing of the imaging for morphologic, atmospheric, and geologic process studies; stereo imaging for 3-D site characterization and rover mobility issues; and multispectral imaging for rapid characterization of the mineralogy and color properties of the scene around the rover. The engineering function of the Pancams is to image the sun and determine its orientation. This information, plus data from accelerometers that measure local vertical, is used to establish an inertial referenced coordinate system. Since Mars lacks an appreciable magnetic field, this system is used in lieu of a reliable magnetic compass. The coordinate system, including its knowledge of north, is then used for both navigation and pointing of the high gain antenna [2].

The Pancams will be mounted on a deployable mast, 50–70 cm above the rover deck. Both cameras will have identical optics with a 16°×16° square field of view (FOV). Horizontal separation of 28 cm and small toe-in provide adequate parallax for stereo imaging. The optical design allows the Pancams to maintain focus from infinity to within 1.5 m of the rover, with an acceptable amount of defocus at closer ranges. In addition, each camera will have a small 8-position filter wheel to allow multispectral sky imaging and surface mineralogical studies in the 400- to 1100-nm wavelength region.

The attitude of the rover is based on measurements from two vector instruments: (1) accelerometers that determine the vector towards the center of gravity of Mars and (2) Pancam solar images that determine the vector to the Sun. In the case that the Sun is overhead, and the accelerometer and Sun vector measurements are close to anti-parallel (i.e., parallel, but pointing in opposite directions), it is not possible to determine the attitude of the rover in all three axes. Because of this, information on the missing axis is obtained by taking two solar measurements 10 minutes apart, resulting in a nominal spacing of 2.5°. With these two solar measurements, the attitude of the rover can then be determined in all three axes, and an inertial referenced coordinate system can be established[3] [3].

The relatively narrow FOV of the Pancams means that initial acquisition of the Sun requires a sky search by rotating them on their gimbal. After the initial solar acquisition, the approximate direction of the Sun is known, a priori, and the Sun can nominally be acquired in a Pancam FOV without a sky search.

---

[3] Small measurement errors result in large heading errors when the Sun is overhead. Therefore, this demands much higher accuracy measurements than for the single measurement case in order to realize the same heading accuracy.

The right and left camera solar filters are different. One is a narrowband filter at a wavelength of 440 nm while the other has a narrowband filter at 880 nm. The different filters also enable studies of the atmospheric spectral absorption and scattering. Both narrow band filters has been coated with a reflective ND5 coating.

The Pancam uses a space qualified charge coupled device (CCD) image detector, by Mitel. It is a front side illuminated, frame transfer type with 12 × 12 μm pixels, with a 1024 × 1024 pixel image register and a 1024 × 1024 pixel storage register. The full well capacity of the pixels is larger than 150,000 electrons and the dark current is specified at less than 1.5 nA/cm^2 by end of the mission at 27° C. The electronics allows exposure times of the camera from 0 to >30 seconds in steps of 5 msec. The frame transfer time is 5 msec and the read noise is less than 50 electrons. The signal is digitized with a 12-bit A/D converter, with a rate of >200,000 pixels/sec resulting in a frame read time of ~5 sec. The camera can also do binning in 4 × 1 pixel boxes and can be commanded to read a set of adjacent rows, instead of the full frame. A drawing of the Pancam is shown in Figure 2. An electronic block diagram of the camera is shown in Figure 3. Finally, Figure 4 shows a diagram of the optics [4].

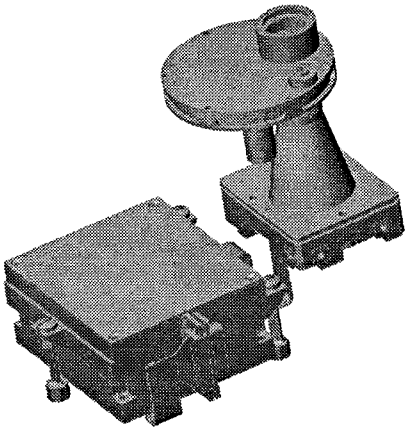

Figure 2. Computer drawing of the MER Pancam

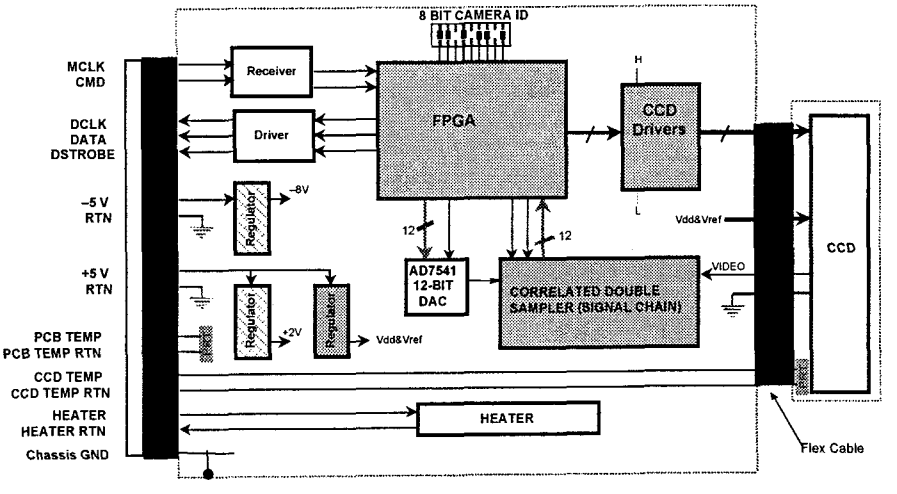

Figure 3: Electronics block diagram of Pancam

Figure 4. Optical design of the Pancam

4. RADIOMETRY

On the Pancams, the sun is imaged through a narrowband filter of 440 nm (left camera) or 880 nm (right camera). The Sun is very bright and a CCD camera is very sensitive to light. Therefore the narrowband filters have been coated with a reflective ND5 coating to attenuate the sun signal. This section discusses the radiometric calculations.

The Sun is a black body radiator with a surface temperature of ~5800° K. The distance from the Sun to Mars is 1.52 AU. Therefore the power density at Mars is ~562.7 W/m^2. The focal length of the lens is 42.68 mm and the F/# is 20. This means that the lens aperture is 2.1 mm and the aperture area is 3.6 mm^2. The solar flux intercepted by the lens is then 2 mW. The spectral solar flux intercepted by the optics is shown in Figure 5.

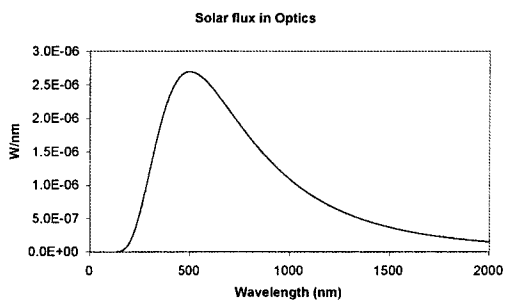

Figure 5. The solar flux intercepted by the optics

The spectral transmission of the narrow band pass filter that is ND coated is shown in Figure 6.

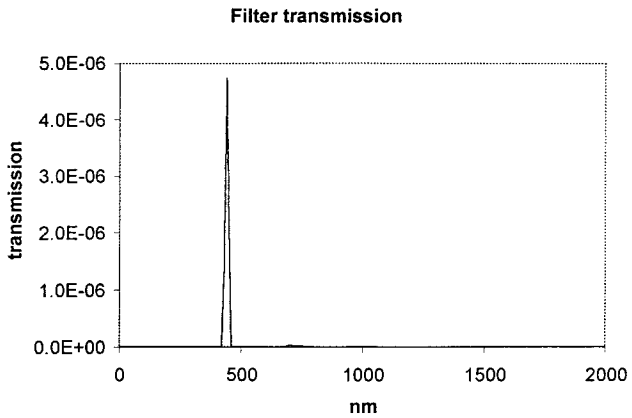

Figure 6. The spectral transmission of band pass filter and the ND coating

At Mars, there is a significant amount of dust suspended in the atmosphere. Therefore, only a fraction of the light is transmitted to the surface of Mars. The dust primarily absorbs light in the blue end of the spectrum. The attenuation depends on the location, time of the year and weather conditions. G. De Vaucouleurs [5] estimates that ~80% of the light is transmitted at 440 nm. 80% corresponds to an optical depth of _=0.22 ($1/e^{0.22}$=0.8). During severe dust storms _ can increase to 5.

The optical design of the Pancam lens includes 5 lenses (Figure 4). That is a total of 10 lens surfaces. Assuming that 98% of the light is transmitted though a lens surface, then only 0.98^{10}=82% of the light is transmitted though the lens.

Multiplying Figure 5 and Figure 6 can calculate the incident number of photons on the focal plane. Also the transmission of the atmosphere (0.8) and the transmission in the lens (0.82) must be multiplied. The result is shown in Figure 7.

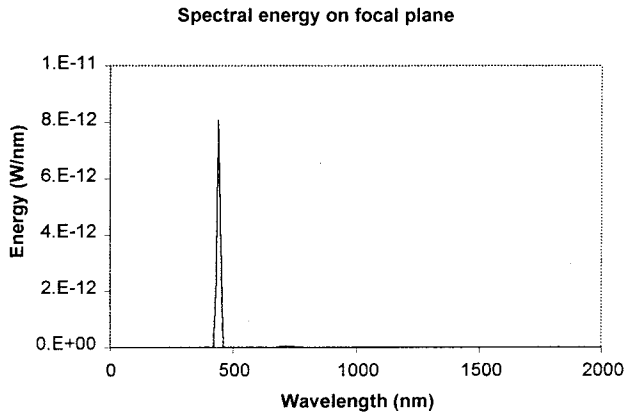

Figure 7. Spectral energy incident on the focal plane

Only a fraction of the photons get converted into photoelectrons. This is called the quantum efficiency of the image detector. The quantum efficiency for the Mitel CCD detector is shown in Figure 8.

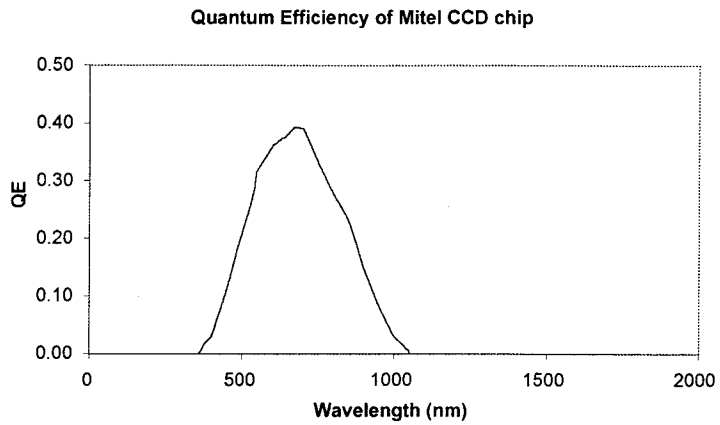

Figure 8. Quantum efficiency for the Mitel CCD chip

Multiplying Figure 7 and Figure 8 and dividing with the specific photon energy will determine how many photoelectrons are detected at different wavelengths. This is done in Figure 9.

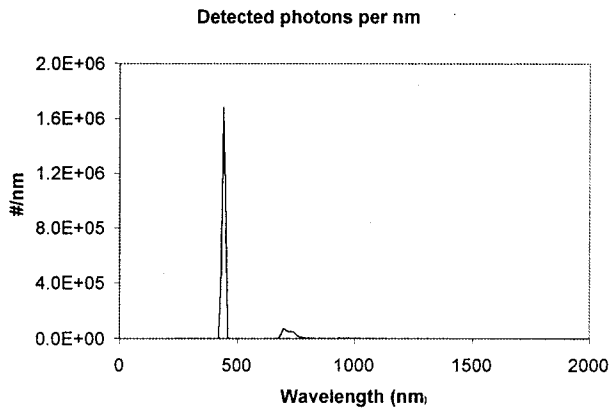

Figure 9. The number of detected photons at the different wavelengths

By adding all wave lengths in Figure 9, it is determined that the Sun generates a total of $3.4 \cdot 10^7$ photoelectrons on the focal plane per second. The Sun on Mars will have a diameter on ~22 pixels in the Pancam. This is equivalent to an area of ~380 pixels. This means that the Sun generates ~90000 photoelectrons per pixel per second.

The full well of a pixel is >150000 photoelectrons. Unfortunately, in some cases (warm temperature and end of mission) the dark current can be as high as 67500 photoelectrons. This means that the available full well is only 150000-67500=82500 photoelectrons. Since the sun generates 90000 photoelectrons per second, an exposure time of 0.5 seconds were selected for the 440 nm band pass filter.

The other Pancam has a band pass filter of 880 nm. Similar calculations on this filter shows that the Sun generates $2.1 \cdot 10^8$ photoelectrons per pixel in this camera. Consequently, the recommended exposure time for this camera is 100 ms.

5. ALGORITHMS

The distance from Mars to the Sun is 1.52 AU. Therefore the angular size of the Sun at Mars is only 0.35°. This is equivalent to a circular diameter of ~22 pixels in each Pancam. The readout time for the camera is 5 seconds, during which time the CCD dark current increases linearly over the image. A simulated image of the Sun is depicted in Figure 10. The effects of dark current are scaled for maximum temperature at end-of-life.

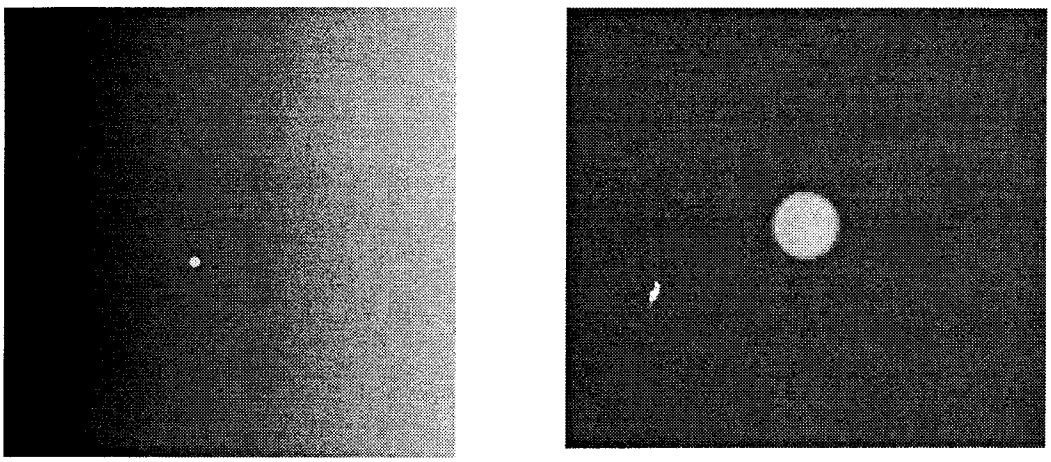

Figure 10. Simulated Pancam image of the Sun and close up of the Sun

When a solar image is acquired, the dark current is estimated as a linearly increasing function of the row averages. The dark current row averages are calculated as:

$$D(j) = \frac{1}{1024}\sum_{i=1}^{1024} I(i,j) \tag{1}$$

Where I(i,j) is the original image intensity. The D function is a linear increasing function of row number. Therefore, a linear function is fitted to the dark current row averages. The slope of the function is (same function used in the Microsoft Excel function slope):

$$slope = \frac{1024 \cdot (\sum_{i=1}^{1024} i \cdot D(i)) - \sum_{i=1}^{1024} i \cdot \sum_{i=1}^{1024} D(i)}{1024 \cdot \sum_{i=1}^{1024} i^2 - (\sum_{i=1}^{1024} i)^2} \tag{2}$$

The background subtracted image is:

$$I_2 = I - slope \cdot \begin{pmatrix} 0 & 1 & \cdots & 1023 \\ 0 & 1 & \cdots & 1023 \\ \cdots & \cdots & \cdots & \cdots \\ 0 & 1 & \cdots & 1023 \end{pmatrix} \tag{3}$$

The dark current image is subtracted from the original image. As an example, this is shown in Figure 11.

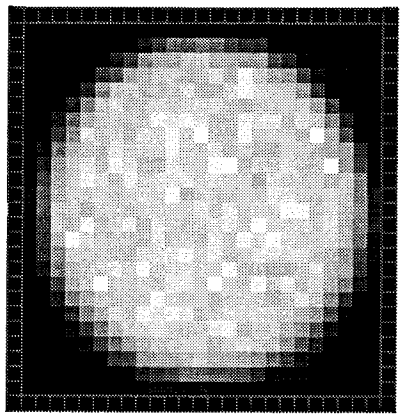

Figure 12. The window used to calculate the centroid, and the border pixels of the window indicated with red squares

The brightness (DN) and the centroid (x_{cm}, y_{cm}) are calculated from the background-subtracted pixels in the window as shown in (4)-(6) [6-7].

$$DN = \sum_{i=ROIstart}^{ROIend} \sum_{j=ROIstart}^{ROIend} image(i,j) \tag{4}$$

$$x_{cm} = \sum_{i=ROIstart}^{ROIend} \sum_{j=ROIstart}^{ROIend} \frac{i \cdot image(i,j)}{DN} \tag{5}$$

$$y_{cm} = \sum_{i=ROIstart}^{ROIend} \sum_{j=ROIstart}^{ROIend} \frac{j \cdot image(i,j)}{DN} \tag{6}$$

As observed in Figure 11, it can be difficult to find the optimal position of the window for the centroid calculations. Therefore, the centroiding calculation is iterated twice. First time it is done as previously described. Second time, the window will be placed at the position of where the first iteration calculated the centroid.

The sensor model is a mathematical equation that relates centroid coordinates to the orientation of the Sun in an instrument based coordinate system. The sensor model is used to transform the centroid coordinates into a sun vector. For this model there are established two different coordinate systems (CS). 1) A CCD chip based right hand CS that has x and y axes aligned with the row and column axes of the CCD chip and the z axis pointing towards the targets, and 2) an alignment cube right hand CS that is aligned with the alignment cube surfaces. The model only includes 6 unknown camera parameters. Those are: the focal length, F (nominal value: 42.68 mm), the intersection of boresight with the focal plane (x_0, y_0) (nominal value: (512,512)), and the rotation from the focal plane coordinate system to the alignment cube coordinate system (3 different Euler angles, _, _, _) (nominal value: 0°, 0°, 0°). The calibration that determines the precise values of these 6 parameters will be discussed in detail in Section 7 of this paper.

In a simple pinhole model, the equations for transforming the centroid coordinates on the focal plane into unit vectors in a CCD based CS are:

$$S_1 = \begin{pmatrix} i \\ j \\ k \end{pmatrix} = \begin{pmatrix} \cos(atan2(x-x_0, y-y_0)) \cdot \cos(\frac{\pi}{2} - atan(\sqrt{\left(\frac{x-x_0}{F}\right)^2 + \left(\frac{y-y_0}{F}\right)^2})) \\ \sin(atan2(x-x_0, y-y_0)) \cdot \cos(\frac{\pi}{2} - atan(\sqrt{\left(\frac{x-x_0}{F}\right)^2 + \left(\frac{y-y_0}{F}\right)^2})) \\ \sin(\frac{\pi}{2} - atan(\sqrt{\left(\frac{x-x_0}{F}\right)^2 + \left(\frac{y-y_0}{F}\right)^2})) \end{pmatrix} \tag{7}$$

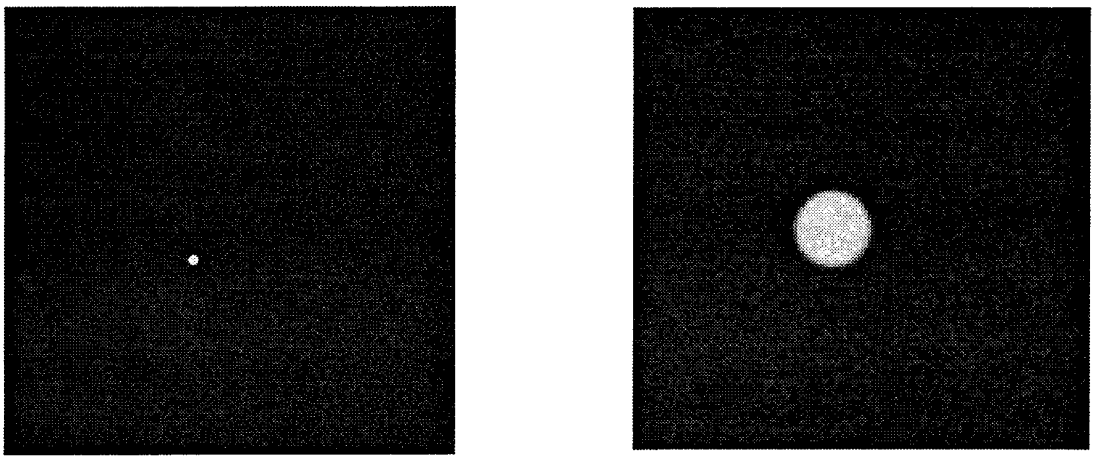

Figure 11. The background subtracted image from Figure 10

Subsequently, a window of 27 × 27 pixels is moved over the entire image. At all positions, the average pixel value of the border of the window is calculated. This value is subtracted from all pixels inside the window. The sum of the background subtracted pixels is added and the value is recorded. This is done for all positions on the image and the position with the highest value is assumed to contain the Sun if it is above a given threshold value.

This algorithm is chosen because it favors bright spots with the approximate size of the Sun. The reason for this is that small spots will not add up to the same sum as the sun image containing ~380 bright pixels. On the other hand, larger objects (or non circular objects with a larger circumference to area ratio) cannot be contained completely inside the 27 x 27 pixels box. Therefore, some of the bright pixels will be at the edge of the window and be part of the average pixel value of the border. This will be subtracted from all pixels inside the window. As an example, the sum of all pixels inside the window minus the average pixel value on the border is shown in Figure 12 for the picture shown in Figure 11.

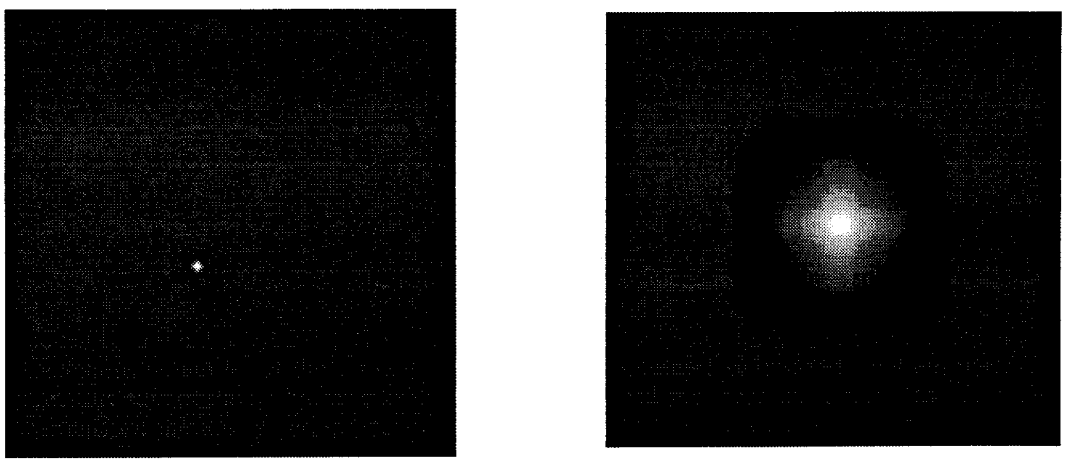

Figure 11. The sum of the pixels inside the window minus the average pixel value on the border of the window

When the position of the brightest window is identified, the centroid of the solar image is then calculated. Again, the average pixel value on the border is calculated as shown in Figure 12 and subtracted from all pixels in the window.

Where (x,y) is the focal plane coordinate, (x_0,y_0) is the intersection of the focal plane and the optical axis, F is the focal length of the optical system, atan2 is four quadrant inverse tangent and S_1 is a unit vector pointing towards the Sun in a CCD based CS.

The 3 Euler angles (_, _, _) are converted into a direction cosine matrix A [8]. The unit vector of the Sun in a CCD based CS is then transformed into the alignment cube based CS. The equations for transforming the unit vector are:

$$S_2 = A \cdot S_1 \tag{8}$$

The distortion of the optics is small (< 0.01%). Therefore, a simple pinhole model has been used. If higher accuracy is required, an optical distortion correction polynomial can also be added to the equations. However, it is not anticipated to be necessary.

6. THE COELOSTAT FACILITY

The Table Mountain Observatory is located in Wrightwood, California. It houses a coelostat used for sun sensor and camera testing. The coelostat is a two-mirror device controlled by analog electronics which tracks sidereal motion and redirects sunlight into a room where devices under test are exposed to this constant sunlight. Figure 13 shows a photograph of the coelostat seen from the outside and Figure 14 shows a block diagram of the facility. .

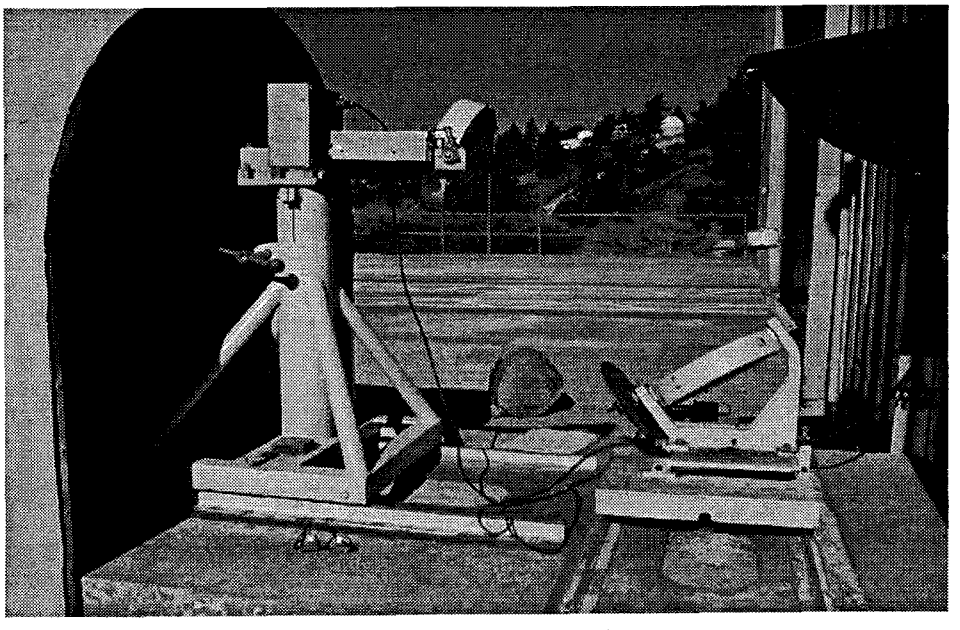

Figure 13. TMF coelostat mirrors

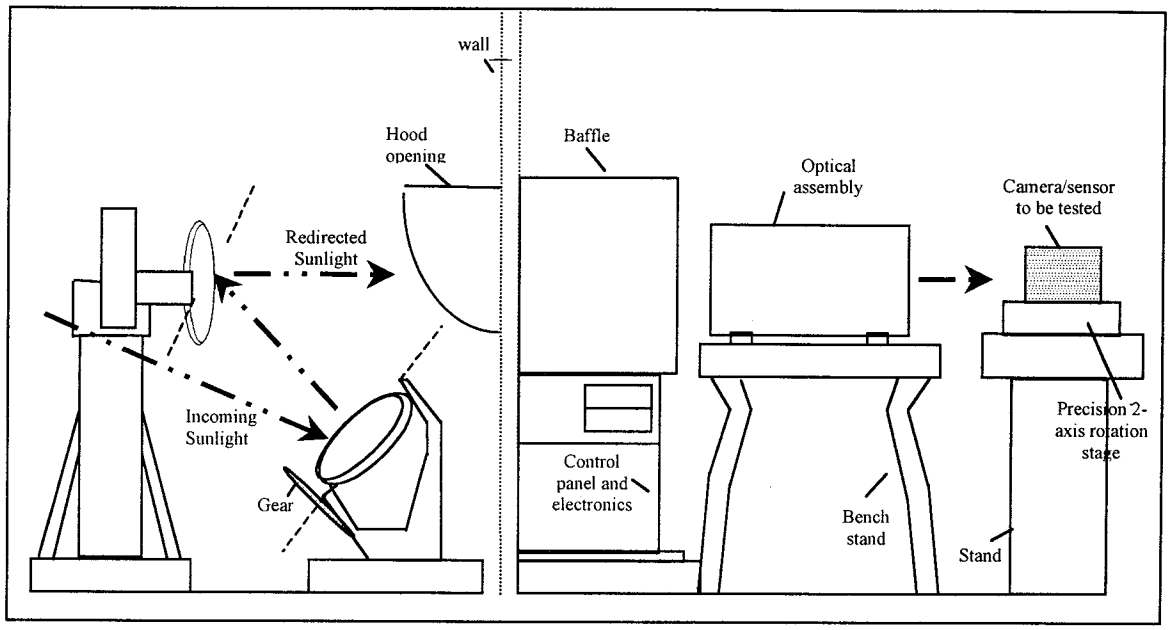

Figure 14. Sketch of TMF coelostat facility as configured for testing

The distance from the Sun to Mars is 1.52 AU. Therefore the angular size of the Sun at Mars is only 0.35° compared to 0.53° here at Earth. As it was explained in the algorithm section a window on 27x27 pixels is used to detect the sun. The algorithm will therefore not operate if the Sun is much larger than anticipated. Therefore the sunlight needs to be converted so it looks like on Mars. This is done in the "optical assembly" shown in Figure 14. The "optical assembly" is shown in details in Figure 15. Two lenses mounted in each end of an optical tube with different focal lengths. This will change the beam convergence. Unfortunately, there are losses on the mirror surfaces and in the lenses. It is only anticipated that the optical setup will be able to reach a power density of 410 W/m^2, compared to the 560 W/m^2 at Mars.

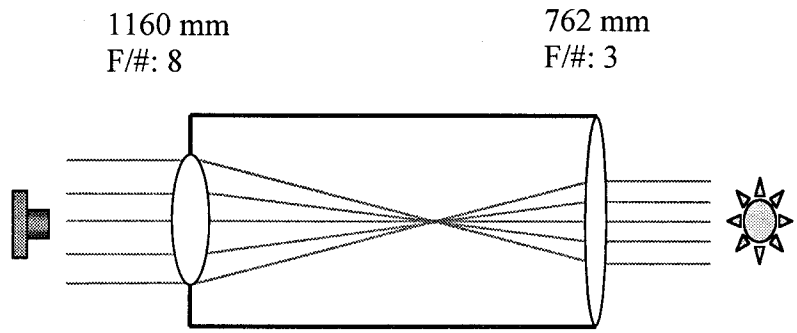

Figure 15. The optical assembly changing the beam divergence

An experiment was conducted utilizing a commercial CCD camera to assess the stability of the coelostat. The camera acquired three pictures per minute from 10am to 3:30pm while mounted in the path of redirected sunlight. The centroids of the sun images were calculated for all images and are shown in Figure 16 and Figure 17. The standard deviations of the centroids were 2.7 and 1.3 arcseconds respectively. The values obtained were more than an order of magnitude better than the required accuracy of the Pancam.

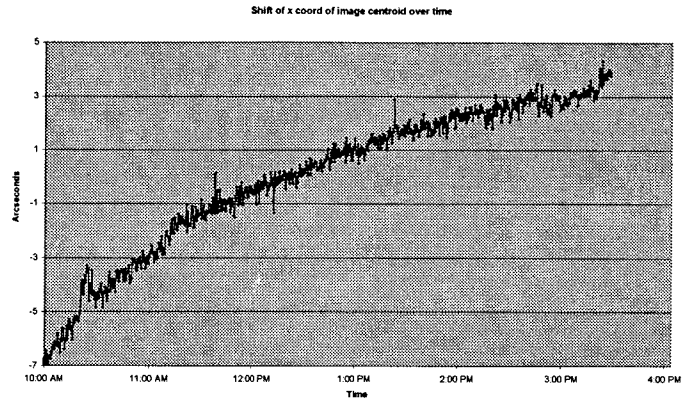

Figure 16. Plot of centroid x-coordinate over time

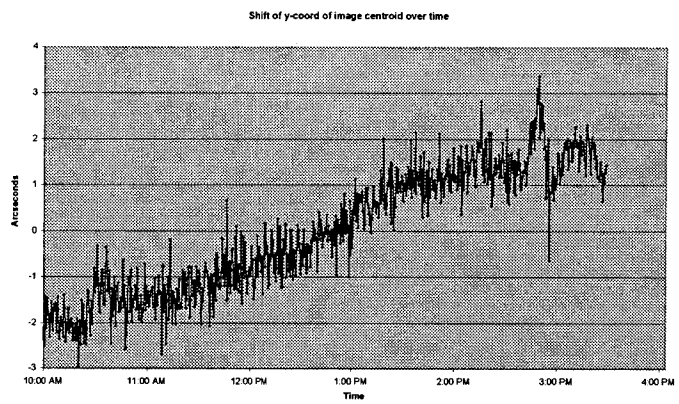

Figure 17. Plot of centroid y-coordinate over time

Based on the experiment, it is concluded that the coelostat is accurate enough to do the Pancam calibration.

7. CALIBRATION

The Pancam will be calibrated at the Table Mountain Observatory solar tracking coelostat facility. The output beam of the coelostat has a constant orientation, regardless of the orientation of the real Sun. The Pancam will be mounted on a precision 2-axis gimbal in the output beam of the coelostat. The gimbal will position the Pancam in a large number of orientations (289), where solar images will be acquired. A sketch of the 2-axis gimbal with the Pancam is shown in Figure 18. The dashed lines indicate the two axis of rotation.

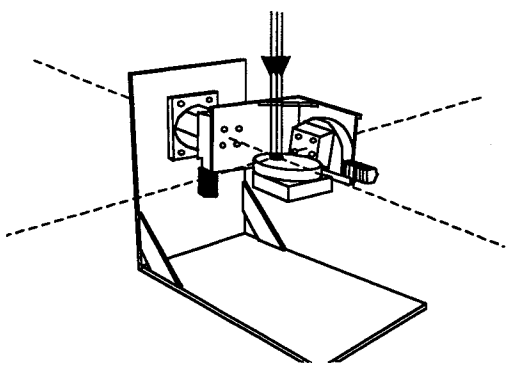

Figure 18. A sketch of the 2-axis gimbal used to calibrate the sun sensor

In the equations a right hand Cartesian coordinate system is used. The Gimbal is rotated around the x-axis and y-axis. The rotations are defined as shown in Figure 19 [9].

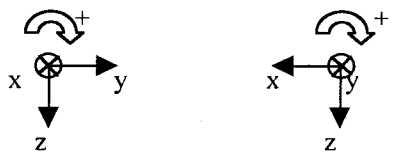

Figure 19. The definition of the gimbal rotations

Rotation matrix for rotation α around the x-axis:

$$A_x = \begin{pmatrix} 1 & 0 & 0 \\ 0 & \cos\alpha & -\sin\alpha \\ 0 & \sin\alpha & \cos\alpha \end{pmatrix} \tag{9}$$

Rotation matrix for rotation β around the y-axis:

$$A_y = \begin{pmatrix} \cos\beta & 0 & \sin\beta \\ 0 & 1 & 0 \\ -\sin\beta & 0 & \cos\beta \end{pmatrix} \tag{10}$$

Rotation matrix for rotation β around y axis and then α around x axis:

$$A_{xy} = A_x \cdot A_y = \begin{pmatrix} \cos\beta & 0 & \sin\beta \\ \sin\alpha\sin\beta & \cos\alpha & -\sin\alpha\cos\beta \\ -\cos\alpha\sin\beta & \sin\alpha & \cos\alpha\cos\beta \end{pmatrix} \tag{11}$$

Vector v represents the orientation of the sun, when α and β are zero. This is shown in Figure 20.

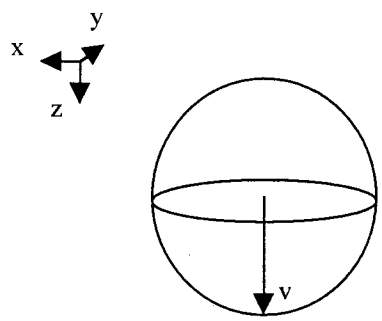

Figure 20. A vector representing the sun, when the gimbal angles are zero

The sun vector-representing zero angles:

$$v = \begin{pmatrix} 0 \\ 0 \\ 1 \end{pmatrix} \tag{12}$$

The sun vector (v), can now be calculated as:

$$v = A_{xy} \cdot v = \begin{pmatrix} \cos\beta & 0 & \sin\beta \\ \sin\alpha\sin\beta & \cos\alpha & -\sin\alpha\cos\beta \\ -\cos\alpha\sin\beta & \sin\alpha & \cos\alpha\cos\beta \end{pmatrix} \cdot \begin{pmatrix} 0 \\ 0 \\ 1 \end{pmatrix} = \begin{pmatrix} \sin\beta \\ -\sin\alpha\cos\beta \\ \cos\alpha\cos\beta \end{pmatrix} \tag{13}$$

It is assumed that the distance from the aperture to the focal plane is 1. The projection is sketched in Figure 21. The coordinates on the focal plane are the intersection of the sun vector and a xy plane.

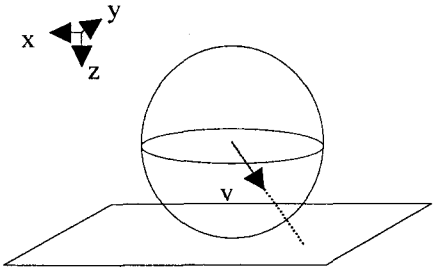

Figure 21. The intersection of the sun vector and a xy plane

The z coordinate of the focal plane is 1. The intersection between the sun vector and the focal plane is therefore:

$$\begin{pmatrix} x \\ y \end{pmatrix} = \begin{pmatrix} \frac{x}{z} \\ \frac{y}{z} \end{pmatrix} = \begin{pmatrix} \frac{\sin\beta}{\cos\alpha\cos\beta} \\ \frac{-\sin\alpha\cos\beta}{\cos\alpha\cos\beta} \end{pmatrix} = \begin{pmatrix} \frac{\tan\beta}{\cos\alpha} \\ -\tan\alpha \end{pmatrix} \tag{14}$$

An image of the aperture centroids as they would move on the focal plane is shown graphically in Figure 22. The angles _ and _ are varied from –8° to 8° in steps of 1°.

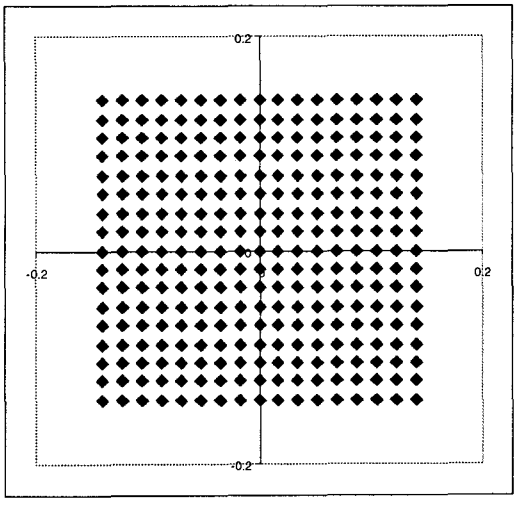

Figure 22. The position of the aperture centroid on the focal plane

In the calculations, it has been assumed that the distance between the aperture and the focal plane is 1. In the following, it is assumed that the distance is F, where the unit of F is units of the pixel size (12 microns). The scenario is shown in Figure 23

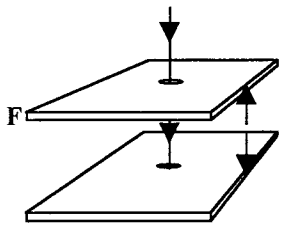

Figure 23. The Pancam sensor model. The top plate is a mask with one aperture and the bottom plate is the detector array. The distance between the plates is F. The unit of F is in pixels

The coordinates of the sun on the focal plane as a function of the gimbal angles can be written as:

$$\begin{pmatrix} x \\ y \end{pmatrix} = \begin{pmatrix} F \cdot \dfrac{\tan\beta}{\cos\alpha} \\ -F \cdot \tan\alpha \end{pmatrix} \tag{15}$$

The focal plane may not be completely aligned with the sun coming from zenith. The sun not coming directly from zenith could cause this. It can also be caused by the gimbal zero angles not being aligned with the focal plane. In Figure 24 is shown the situation, where the focal plane is offset in two orthogonal axes.

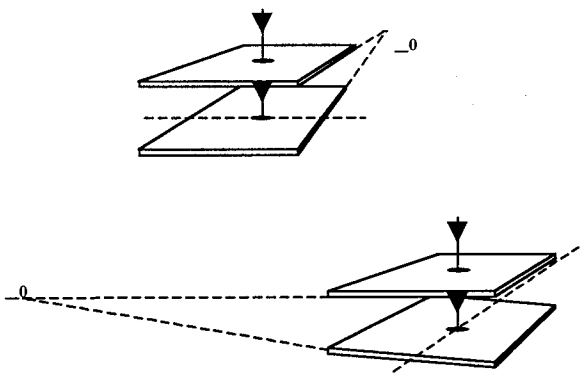

Figure 24. A sketch of the Pancam sensor system. In the two sketches an angle offset in two orthogonal axes are shown.

Assuming that $\__0$ and $\__0$ are the offsets, the equations for the aperture centroid, as a function of the two gimbal angles, are then:

$$\begin{pmatrix} x \\ y \end{pmatrix} = \begin{pmatrix} F \cdot \dfrac{\tan(\beta-\beta_0)}{\cos(\alpha-\alpha_0)} \\ -F \cdot \tan(\alpha-\alpha_0) \end{pmatrix} \tag{16}$$

The detector plane may also have been rotated around an axis orthogonal to the plane. This angle is called _. This is sketched in Figure 25.

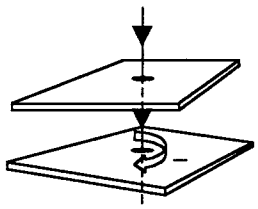

Figure 25. The Pancam sensor system. In the Figure the image detector has been rotated an angle _ orthogonal to the image detector plane.

Utilizing a normal two dimensional coordinate rotation results in the following the equations for the aperture centroid:

$$\begin{pmatrix} x \\ y \end{pmatrix} = \begin{pmatrix} F \cdot \frac{\tan(\beta - \beta_0)}{\cos(\alpha - \alpha_0)} \cdot \cos\phi - F \cdot \tan(\alpha - \alpha_0) \cdot \sin\phi \\ -F \cdot \frac{\tan(\beta - \beta_0)}{\cos(\alpha - \alpha_0)} \cdot \sin\phi - F \cdot \tan(\alpha - \alpha_0) \cdot \cos\phi \end{pmatrix} \tag{17}$$

Until now, it has been assumed that the aperture centroid intersects the image detector in the coordinate (0,0). This will not be the case. The equivalent pinhole will be placed over approximately the center of the CCD chip. This is sketched in Figure 26. The intersection is called (x_0,y_0).

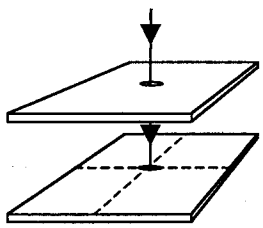

Figure 26. The Pancam sensor system. In this Figure the intersection of the aperture centroid and the image detector has been illustrated with a dotted cross hairs

The new equations for the aperture centroid, as a function of the two gimbal angles will then be:

$$\begin{pmatrix} x \\ y \end{pmatrix} = \begin{pmatrix} F \cdot \frac{\tan(\beta - \beta_0)}{\cos(\alpha - \alpha_0)} \cdot \cos\phi - F \cdot \tan(\alpha - \alpha_0) \cdot \sin\phi - x_0 \\ -F \cdot \frac{\tan(\beta - \beta_0)}{\cos(\alpha - \alpha_0)} \cdot \sin\phi - F \cdot \tan(\alpha - \alpha_0) \cdot \cos\phi - y_0 \end{pmatrix} \tag{18}$$

During the data taking, 289 measurements will be acquired, by sweeping both gimbal angles from –8° to 8° in steps of 1°. This vector set of angles is called _ and _. For each measurement, a set of observed (x,y) centroids on the focal plane will be observed. The four vectors are:

$$\underline{\alpha} = \begin{pmatrix} \alpha_1 \\ \alpha_2 \\ \cdot \\ \alpha_{289} \end{pmatrix} \quad \underline{\beta} = \begin{pmatrix} \beta_1 \\ \beta_2 \\ \cdot \\ \beta_{289} \end{pmatrix} \quad \underline{x_m} = \begin{pmatrix} x_{m,1} \\ x_{m,2} \\ \cdot \\ x_{m,289} \end{pmatrix} \quad \underline{y_m} = \begin{pmatrix} y_{m,1} \\ y_{m,2} \\ \cdot \\ y_{m,289} \end{pmatrix} \tag{19}$$

There are only 6 unknowns. They are $\__0$, $\__0$, _, x_0, y_0 and F. We want to find a solution that minimizes the squared distance between the calculated and measured aperture centroids. Therefore, we want to minimize the following:

$$\sum_{i=1}^{441} \left(F \frac{\tan(\beta_i - \beta_0)}{\cos(\alpha_i - \alpha_0)} \cos\phi - F \tan(\alpha_i - \alpha_0) \sin\phi - x_0 - x_{m,i}\right)^2 + \left(-F \frac{\tan(\beta_i - \beta_0)}{\cos(\alpha_i - \alpha_0)} \sin\phi - F \tan(\alpha_i - \alpha_0) \cos\phi - y_0 - y_{m,i}\right)^2 \tag{20}$$

This can be solved utilizing Matlab or the Solver in Excel.

At the same time of the calibration, a theodolite with an autocollimator must also be used. The instrument reads the surfaces of the alignment cube and establishes a coordinate system. The theodolite also looks at the Sun (with a filter) and determines the bearing of the Sun. A number of these measurements are made at different gimbal orientations and are used to establish the rotation from the CCD based CS to the alignment cube based CS [3].

8. ERROR BUDGET

As described in Section 3, the Pancam needs to determine the orientation to the Sun accurately to point the high gain antenna towards Earth. The overall error budget has Pancam allocations as shown in Table 3.

Table 1. Pancam accuracy requirements (1 axis, 3_)

Absolute Error at boresight	0.2°
Absolute error at edge of FOV	0.27°
Relative systematical error over 2.5°	0.05°

To asses the accuracy of the Pancam an error budget is constructed. Initially the centroiding accuracy is simulated. Generating random Sun images does this. The Sun images are created using the sequence of procedures as outlined in Figure 27.

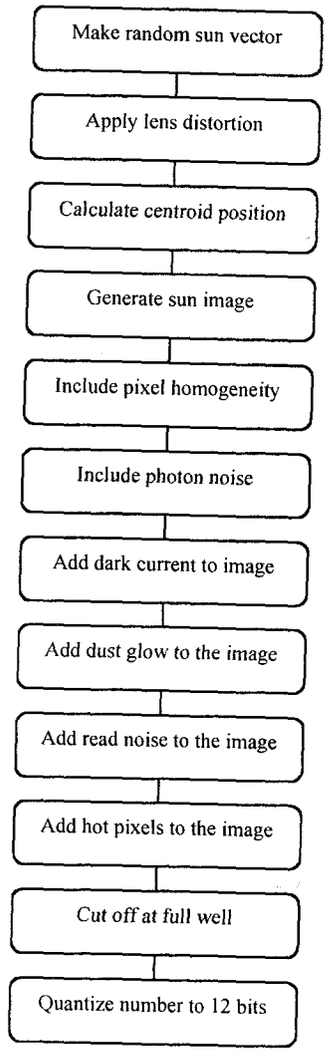

Figure 27. The sequence of procedures for generating an artificial Sun image

Below are the different steps for generating an artificial Sun image are described:

Make random sun vector: A random sun vector is generated. Care must be taken so the unit vectors are generated isotropically.

Apply lens distortion: The lens distortion in the optics is minimal (0.1%). However, it is included in generating artificial Sun images. The lens distortion has been obtained from the Zemax program for different angles and is interpolated.

Calculate centroid positions: The sun vector is transformed into a centroid using a simple pinhole camera model. The camera parameters are the nominal values.

Generate Sun image: A sun image is generated. The point-spread function from Zemax is convolved with a bright circle with the size of the Sun. The resolution of the convolved Sun image has a resolution of 1/100 of a pixel. This is resampled to a resolution of 1 pixel and superimposed on a completely black image.

Include pixel homogeneity: Not all pixels have the same sensitivity to photons. In the simulations a pixel in homogeneity of 2% was used.

Include photon noise: The number of photons follows a Poison distribution. Therefore noise is added according to this.

Add dark current to image: The dark current at the highest temperature and at end of the mission is specified to less than 1.5 nA/cm^2. The pixel size is 12 _m x 12 _m. Therefore 13500 photoelectrons are generated a second in each pixels. The image takes 5 seconds to read out. Therefore dark current will increase linearly over the image from ~0 photoelectrons to ~67500 photoelectrons. Statistical noise following a Poisson distribution is also added to the dark current. Finally, the dark current is not uniform. Therefore also a 2% dark current non-uniformity is added to the dark current before it is added to the camera image.

Add dust glow to the image: Mars is a very dusty place. Dust may be deposited on the outer lens surface and the sun may scatter in the deposited dust. Fortunately, the scattered light will not be in focus and the size of the dust grains will be small (1 micron) compared to the size of the aperture (2.17 mm). Therefore the dust will only show up as a background glow. The front lens (filter) has an area of 95mm^2 and receives 53.3 mW of solar flux. A large uncertainty is associated with the dust deposition. However, for surfaces looking up (the Pancam will only look up, when staring at the Sun) the optical transmission will decrease 0.3% per day [10]. A conservative estimate is there will be 10% transmission losses due to dust at end of the mission. A conservative assumption would be that all this light is forward scattered into the lens and homogeneous distributed over the pixels. It was previously shown that 2 mW generates $3.7 \cdot 10^7$ photoelectrons. Therefore 10% of 53.3 mW will generate $9.1 \cdot 10^7$ photoelectrons per second. This signal is homogeneously distributed to all pixels (1 million) so each pixel receives 86.4 photoelectrons per second. The first pixel that is read out receives only the exposure time dust glow while the last pixel receives ~432 photoelectrons. The dust glow signal follows a Poisson distribution, which is added to the signal.

Add read noise to the image: A read noise of 50 photoelectrons is added to all pixels.

Add hot pixels to the images: A few hot pixels may be added to the image. The position and brightness is random. Up to 10 hot pixels are added to the Sun image.

Cut off at full well: Make sure that no more than 150,000 photoelectrons are in any pixel.

Quantize number to 12 bits: Truncate numbers so resolution of the number of photoelectrons is 4096 (12-bit).

There exist a number of other small phenomena that add noise to the centroiding. Examples are Charge Transfer Efficiency (CTE) and frame transfer smear. CTE is when a small fraction of the charge is left behind in a pixel during shifting the image out. Frame transfer smear occurs because the shifting from the exposure area to the storage area takes a finite time (5 micro seconds). Both phenomena result in a tail after the sun. This results in a centroid shift of the Sun. However, none of the effects is larger than 1/1000 of a pixel and is therefore not included in this simulation.

Ghost images are yet another phenomena that may shift the centroids. It typically occurs close to the optical boresight. The image of the Sun hits the focal plane and a percentage of the photons are reflected back to the optics. In the optics the photons gets reflected at the reflective ND coating and bounce back on the focal plane close to the position of the original image. Stray light analysis has been performed on the lens and it has shown that the centroid shift will be less than 1/1000 of a pixel.

After this sequence of procedures has been applied, a typical artificial Sun image looks like shown in Figure 10.

When the artificial image is generated, the algorithm described in Section 5 is applied to the image. The resulting Sun vector is compared to the original sun vector and the error is calculated. This sequence was repeated thousands of times and the average error was found to be 0.0016°.

The calibration will not be perfect and there will be some uncertainty in the camera parameter estimates. This has not been included in the simulations at this point. However, it is typically possible to calibrate, so that the camera pinhole residuals (errors) are less than 1 pixel. Also the camera has a huge operating temperature range (-55°C-40°C). Therefore, some thermal expansion of the lens will occur. It is expected that the FOV will change less than X %. The boresight is expected to drift less than X degrees. The overall error budget is shown in Table X

Table 2. Error budget.

	Error at boresight	Error at Edge of FOV	Relative systematical error
Centroiding error	0.002	0.002	0.002
Drift in FOV	?	0	?
Drift of boresight	?	?	?
Calibration residual	0.015	0.015	0
Alignment cube error	0.005	0.005	0
Total	?	?	?

It is observed in Table 2 that the Pancam can determine the orientation of the Sun more accurately than it is required.

9. SUMMARY

This paper has briefly described the Mars Exploration Rovers Mission. One of the cameras on the MER rover is the Pancam. This paper has given a technical description of the Pancam.

One of the functions of the Pancam is to determine the orientation of the Sun. To stare at the sun, the Pancam has a narrow band filter and a ND5 filter. The radiometry calculations have been described in this paper. Also, the algorithm that is used to calculate the centroid and Sun angles has been explained.

The Pancam will be taken to a special coelostat facility and calibrated. The coelostat and the calibration method have been discussed. Finally an error budget for the Pancam was shown.

ACKNOWLEDGMENTS

The authors would like to thank Paul Karlman, JPL for providing Figure 2. Mark Schwochert for providing Figure 3 and Larry Scherr for providing Figure 4.

The research described here was carried out at the Jet Propulsion Laboratory, California Institute of Technology, and was sponsored by the National Aeronautics and Space Administration. References herein to any specific commercial product, process or service by trademark, manufacturer, or otherwise, does not constitute or imply its endorsement by the United States Government or the Jet Propulsion Laboratory, California Institute of Technology.

REFERENCES

[1] Jet Propulsion Laboratory, California Institute of Technology: http://www.jpl.nasa.gov/missions/future/marsexplorationrovers.html, Cited 9/19/2001.

[2] A Eisenman et al: Mars Exploration Rover Engineering Cameras, SPIE Proceedings of International Symposium on Remote Sensing, 17 - 21 September 2001, Toulouse, France.

[3] M.D.Shuster, S.D.Oh: Three-axis attitude determination from vector observations, Journal of Guidance and Control, 4(1): 70-77, Jan.-Feb. 1981.

[4] G.H.Smith, E.C.Hagerott, L.M.Scherr, K.E.Herkenhoff, J.F.Bell III: Optical designs for the Mars '03 rover cameras, Proceedings of SPIE Vol. 4441-14.

[5] G. de Vaucouleurs: Physics of the Planet Mars, Faber and Faber, London, 1954.

[6] Liebe, Carl C; Dennison, Edwin W; Hancock, Bruce; Stirbl, Robert C; Pain, Bedabrata: Active Pixel Sensor (APS) based star tracker, 1998 IEEE Aerospace Conference, Aspen, CO, Mar. 21-28, 1998, Proceedings. Vol. 1 (A98-34386 09-31), p. 119-127.

[7] C.C.Liebe: Star Trackers for Attitude Determination, IEEE AES Magazine June 1995, p.10-16.

[8] James R. Wertz: Spacecraft Attitude Determination and Control, D.Reidel Publishing Company, Dordrecht, Holland.

[9] C.C.Liebe, S. Mobasser: MEMS based sunsensor: Proceedings of IEEE 2001 Aerospace conference.

[10] Geoffrey A. Landis: Mars Dust Removal Technology, *AIAA Journal of Propulsion and Power* Vol. 14, No. 1, 126-128, Jan. 1998.

Allan Eisenman holds both bachelor and Master of Science degrees in electrical engineering from the University of California at Los Angeles. His extensive experience in aerospace engineering includes video display design, analog and digital circuit design, infrared systems engineering, spacecraft science imaging design, complex multi-functional visual and IR focal plane development, space borne video tracking systems, pioneering development of CCD star trackers for spacecraft, celestial sensor development and real sky characterization. Mr. Eisenman is employed at the Jet Propulsion Laboratory in Pasadena, California, as a Senior Staff engineer where he is engaged in the development of advanced

celestial and target tracking sensors for Earth-orbiting and interplanetary spacecraft.

Dr. **Carl Christian Liebe** received the M.S.E.E. degree in 1991 and the Ph.D. degree in 1994 from the Department of Electrophysics, Technical University of Denmark. Since 1997, he has been a member of the technical staff in the Precision Motion Control Systems and Celestial Sensors Group at the Jet Propulsion Laboratory, California Institute of Technology. His current research interests are new technologies and applications for autonomous attitude determination. He has authored/co-authored more than 35 papers.

Ramiro Perez received a B.S.E.E from California State Polytechnic University, Pomona in 2000 and is currently working towards an M.S.E.E. at the University of Southern California. Previous, Mr. Perez worked as a weapon systems analyst for the Department of the Navy. Now an employee of the Jet Propulsion Laboratory, his tasks include modeling of electronic control circuitry, testing and verification of star scanners and analysis of stability and performance of sun-tracking devices. His research interest includes robotics and control.